IEEE Access
Multidisciplinary | Rapid Review | Open Access Journal

Received April 22, 2019, accepted May 30, 2019, date of publication June 10, 2019, date of current version July 2, 2019.

Digital Object Identifier 10.1109/ACCESS.2019.2922135

Mechanism of Temperature's Acting on Electro-Hydraulic Servo Valve

HAO YAN[1, 2], YANG LIU[1], AND LI MA[1]

[1]School of Mechanical, Electronic and Control Engineering, Beijing Jiaotong University, Beijing 100044, China
[2]Key Laboratory of Vehicle Advanced Manufacturing, Measuring and Control Technology, Beijing Jiaotong University, Beijing 100044, China

Corresponding author: Hao Yan (hyan@bjtu.edu.cn)

This work was supported in part by the National Natural Science Foundation of China, under Grant 51775032 and in part by the Foundation of Key Laboratory of Vehicle Advanced Manufacturing, Measuring and Control Technology, Beijing Jiaotong University, Ministry of Education, China.

ABSTRACT To understand temperature's influence on the electro hydraulic servo valve, a theoretical model of describing the detailed mechanism is necessary. For a servo valve experiencing actual working conditions, the temperature variation acts on the performance of the torque motor, which results from drifts of the air gaps' thicknesses, the permanent magnets' reluctances, and the polarization magnetomotive force. And with the temperature variation, the nozzle orifice's size and its flow coefficient also change, which will act on the performance of the valve's pilot hydraulic amplifier. Furthermore, the mechanical characteristics, including the stiffness of the spring tube, the stiffness of the feedback rod and the armature's arm of force, are also related to temperature. Then, considering all these factors, a comprehensive temperature influencing model, referred to as the temperature-induced angular drift model (TAD), is constructed. With fluid, structure and electromagnetic field integrated, this theoretical model reflects complexity of the system and can be characterized by a ninth-order equation with nonlinear time-variant coefficients. On this basis, the routes by which temperature affects the servo valve's control accuracy are investigated. Calculations show that when the temperature ranges from 20°C to 270°C, the valve's control error will exceed 15% of the expected output. Among the temperature's acting routes, the flow coefficient is dominant, the nozzle orifice's diameter and the magnetomotive force are secondary, and others are insignificant. An experiment shows that the TAD model correctly predicts the tendency of the control error caused by temperature's rise, and it will aid in optimizing the servo valve's temperature performance.

INDEX TERMS Hydraulic system, servo valve, temperature influencing model, torque motor.

I. INTRODUCTION

The electro-hydraulic servo valve is a crucial component in hydraulic control equipment. In launch vehicles, the space for the hydraulic system is much limited; hence the reservoir has a small volume and no cooling system is provided. Therefore, the temperature of the hydraulic oil can vary from the atmospheric temperature to over 250°C during a launching session. With the rise of oil temperature, many internal factors of the electro-hydraulic servo valve are affected, resulting in a significant decline of the control precision, which has aroused many researchers' attention.

Researchers have been focusing on issues of temperature and thermal energy in hydraulic systems and elements. Sidders utilized the control volume theory to analyze the hydraulic components' energy exchange [1]. And the thermographic technology was applied to the hydraulic system and a temperature record for different elements was acquired [2]. Then the thermodynamic characteristic of a high-temperature valve for fuel supply was reported by Zeng [3]. In recent years, investigators became interested in the temperature characteristics of electro-hydraulic servo valves. Thermal models of the servo valve were established by Zhu [4] and Y. Li [5]; the heat equilibrium process was simulated and temperatures at different locations were obtained. And Zhao studied the heat-fluid-solid coupling problem and provided visual descriptions on distributions of temperature

The associate editor coordinating the review of this manuscript and approving it for publication was Tongdan Jin.

and deformation in the servo valve [6]. Yin qualitatively analyzed the temperature's influence on the size and fit of mechanical elements in the servo valve and discussed the internal temperature's distribution [7], [8]. Xiao detailedly summarized the temperature influence on the materials, oil's physical properties and the flow field in extreme temperature conditions [9]. X. Zhang and Yin proposed that at different working temperatures the flow coefficients of orifices in the nozzle-flapper servo valve would change [10]. As to the spool valve, Cao established a CFD model of the spool valve to describe the temperature and flow distribution, with consideration of thermal expansion and deformation of solids [11]. Aiming at the spool's jamming caused by throttling heat, J. Zhang derived the relationship between temperature and the spool valve's clamping force [12]. Other researchers established three-dimensional CFD models to analyze temperature distribution and the coupling of flow, solid and heat in the spool valve [13]–[15]. Furthermore, the temperature characteristic of spool material was considered by Zhou [16]. In the aspect of throttling heating mechanism, by the numerical heat transfer (NHF) method W. Li proved that the temperature's rise is mainly caused by the viscous dissipation [17]. In our previous studies, the temperature variable was introduced in modeling the torque motor and the temperature characteristics of the air gap thickness was discussed [18]. And it was proved that the current fluctuation is related to the nonlinear friction caused by temperature's rise [19].

For the temperature characteristics of servo valves, most researches have focused on its certain elements, while there is a lack of theoretical models to describe temperature variation's acting on the final output of the whole valve, which leads to blindness in improving the design and the manufacturing process. Aiming at this issue, the paper will discuss the relationship between temperature variation and performances of various components, including the torque motor, the pilot hydraulic amplifier and the mechanical structure. Then a comprehensive theoretical temperature influencing model will be derived, in which eight internal factors, including air gaps' thicknesses, permanent magnets' reluctances, the polarization magnetomotive force, the nozzle orifice's size, the nozzle's flow coefficients, stiffness of the spring tube, stiffness of the feedback rod and the armature's arm of force, are taken as the main routes by which temperature influences the servo valve. Each route's respective effect on control accuracy is evaluated and comparisons of them are conducted, which can fundamentally explain the mechanism of the temperature's acting on a servo valve. Also, a comprehensive calculation is implemented to predict the control error's general tendency. Finally, the theoretical model is validated by experiments.

The major contributions of the paper are summarized as follows.

(1) A comprehensive theoretical model with consideration of the temperature factor, the temperature-induced angular drift model (TAD), is constructed to describe the temperature influencing mechanism of a servo valve.

(2) Discussions based on the proposed model are conducted to reveal the dominant route of influencing control accuracy.

(3) Experiment methodologies of building temperature conditions and detecting the angular drift of the torque motor are presented to validate the TAD model.

All this is carried out to improve the design of temperature performance of the servo valve.

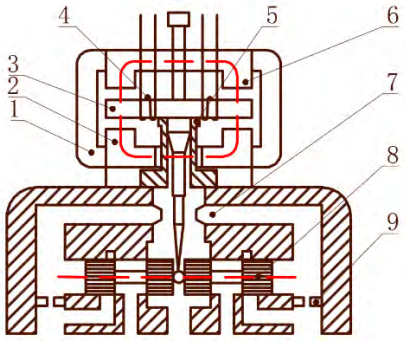

FIGURE 1. Typical electro-hydraulic servo valve. 1 Permanent magnet 2 Lower pole piece 3 Armature 4 Coil 5 Spring tube 6 Upper pole piece 7 Nozzle 8 Spool 9 Fixed orifice.

II. ROUTES OF TEMPERATURE'S ACTING ON THE SERVO VALVE

In this research, temperature is specified to vary between 20°C and 270°C, which covers the temperature condition of the servo valve in launch vehicles. Based on practical experience, the 12# aeronautical hydraulic oil can work with normal performance in the launching session. The typical electro-hydraulic servo valve is composed of a plurality of tiny components, as shown in Figure 1. When the temperature rises rapidly, the torque motor's air gaps, permanent magnet reluctances, the polarization magnetomotive force and the armature's arm of force are firstly affected, and thus the driving torque of the torque motor is disturbed. Besides, the stiffness of the spring tube and the force feedback rod is influenced by temperature, which will change the elastic load of the torque motor. Meanwhile, temperature variation affects the physical properties of hydraulic oil, which causes a change of the nozzle's flow coefficient. In addition, the nozzle orifice's size will also vary. As a result the flow force acting on the flapper and pressures on both sides of the spool are also affected, and these factors can impact on the load torque through the force feedback rod and the spool. Therefore, the drift of the driving torque and the load torque will interfere with the torque motor's output, resulting in a decrease of the servo valve's control accuracy. Thus, a total of eight routes of temperature influencing are considered in this study, analyzed as follows.

III. THEORETICAL MODEL OF TEMPERATURE'S EFFECT ON ELECTRO-HYDRAULIC SERVO VALVE

A. TEMPERATURE INFLUENCING MODELLING OF MAGNETIC FLUX

1) POLARIZATION MAGNETOMOTIVE FORCE

According to previous studies [18], the total polarization magnetomotive force M_0 is

$$M_0 = l_m \frac{B_r}{\mu_r} \tag{1}$$

where B_r is the flux density, l_m is the effective length of the permanent magnet and μ_r is the magnetic permeability.

According to Ref. [20], the relationship between the flux density and temperature is

$$B_r = \left[1 + (T - 20)\,\alpha_{B_r}\right] \cdot (1 - IL)\, B_{r20^\circ\mathrm{C}} \tag{2}$$

and the relationship between the field intensity and temperature is

$$H_c = \left[1 + (T - 20)\,\alpha_{B_r}\right] \cdot (1 - IL)\, H_{c20^\circ\mathrm{C}} \tag{3}$$

where α_{B_r} is the reversible temperature coefficient, IL is the irreversible loss rate, H_c is the field intensity, $B_{r20^\circ\mathrm{C}}$ is the flux density at 20°C, $H_{c20^\circ\mathrm{C}}$ is the field intensity at 20°C and T is current temperature.

Eqs. (2) and (3) show that B_r and H_c have the same variation tendency with respect to temperature. Since μ_r is proportional to the ratio of B_r to H_c, it can be learned that μ_r is hardly affected by temperature variation, which is consistent with the conclusion in Ref. [20]. Thus, ignoring tiny change of the effective length, the relationship between the polarization magnetomotive force and the temperature can be expressed as (4), following from Eqs. (1) and (2).

$$M_0 = \frac{l_m \left[1 + (T - 20)\,\alpha_{B_r}\right](1 - IL)\, B_{r20^\circ\mathrm{C}}}{\mu_r} \tag{4}$$

In the torque motor, the material of the permanent magnet is Al-Ni-Co alloy, with $\alpha_{B_r} = -0.02\%/^\circ\mathrm{C}$, $B_{r20^\circ\mathrm{C}} = 1.27\,\mathrm{T}$ and $IL = 0$. Substituting them into (4) gives

$$M_0 = -0.596(T - 20) + 0.298 \times 10^4 \tag{5}$$

Calculation shows that the polarization magnetomotive force decreases linearly with an increasing temperature at a rate of $-0.02\%/^\circ\mathrm{C}$, which is a different result from Ref. [18]. That means if the temperature reaches 270°C, the polarization magnetomotive force will drop by about 5%, and then its impact should not be neglected.

2) THE AIR GAP'S VARIATION

With the rise of the environment temperature, even if the torque motor's armature is not deflected, the air gap thickness will change because of thermal expansions of the permanent magnet, the pole pieces, the spring tube and the armature, which will lead to the air gap reluctance's variation. Main dimensions of the torque motor are shown in Figure 2. Therefore, the thicknesses of the upper and lower air gaps are

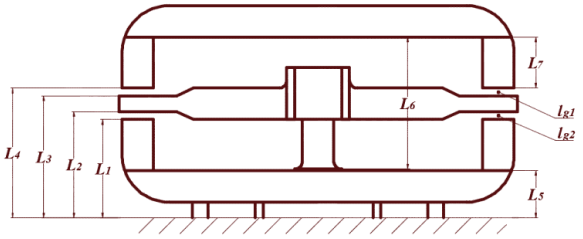

FIGURE 2. Original dimensions of torque motor.

calculated by

$$\begin{cases} l_{g1} = L_4 - L_3 \\ l_{g2} = L_2 - L_1 \end{cases} \tag{6}$$

At the initial temperature of 20°C, the dimensions in Figure 2 are denoted by $L_{ni}(n = 1 \sim 7)$. On the basis of prior research work [18], the expression of L_3 is modified for better accuracy. Then, as the temperature rises, each dimension will expand with respect to the reference plane, that is

$$\begin{cases} L_1 = L_{1i}\,(1 + \alpha_c \Delta T) \\ L_2 = L_{2i}\,(1 + \alpha_s \Delta T) \\ L_3 = L_{2i}\,(1 + \alpha_s \Delta T) + (L_{3i} - L_{2i})\,(1 + \alpha_x \Delta T) \\ L_4 = L_{5i}\,(1 + \alpha_c \Delta T) + L_{6i}\,(1 + \alpha_m \Delta T) - L_{7i}\,(1 + \alpha_c \Delta T) \end{cases} \tag{7}$$

in which α_c, α_s, α_m, and α_x are linear expansion coefficients of the pole pieces, the spring tube, the permanent magnet and the armature, respectively; ΔT is temperature variation.

And at the initial temperature the air gap length is computed as

$$\begin{cases} l_{g1i} = L_{4i} - L_{3i} = L_{5i} + L_{6i} - L_{7i} - L_{3i} \\ l_{g2i} = L_{2i} - L_{1i} \end{cases} \tag{8}$$

Substituting (7) and (8) into (6) yields

$$\begin{cases} l_{g1} = l_{g1i}\,(1 + \alpha_{K1})\,\Delta T \\ l_{g2} = l_{g2i}\,(1 + \alpha_{K2})\,\Delta T \end{cases} \tag{9}$$

where

$$\begin{cases} \alpha_{K1} = \dfrac{(L_{5i} + L_{7i})\alpha_c + (L_{2i} - L_{3i})\alpha_x + L_{6i}\alpha_m - L_{2i}\alpha_s}{l_{g1i}} \\ \alpha_{K2} = \dfrac{l_{g2i}\alpha_s - L_{1i}\alpha_c}{l_{g2i}} \end{cases} \tag{10}$$

α_{K1} and α_{K2} are the comprehensive linear expansion coefficients of the upper and lower air gaps. The material and the expansion coefficient of each element in the torque motor are listed in Table 1, and original values of the dimensions are listed in Table 2.

According to the above formulas, the air gap's temperature characteristic can be calculated, as depicted in Figure 3. With the increase of the temperature, the gaps vary linearly and the thickness of each gap drifts by 6% when the temperature

TABLE 1. The materials and the expansion coefficient of the torque motor.

Component Name	Material name	Linear expansion coefficient $\alpha/10^{-6}(℃)$
Permanent magnets	A1-Ni-Co(α_m)	11
Pole pieces	1J50(α_c)	9.2
Armature	1J50(α_x)	9.2
Feedback rod	3J1(α_f)	12.14
Spring tube	QBe1.9(α_s)	17.6

TABLE 2. Original dimensions of the torque motor.

Parameters	Numerical value	Unit
L_{1i}	7.05	mm
L_{2i}	7.29	mm
L_{3i}	8.62	mm
L_{4i}	8.85	mm
L_{5i}	2.83	mm
L_{6i}	10.24	mm

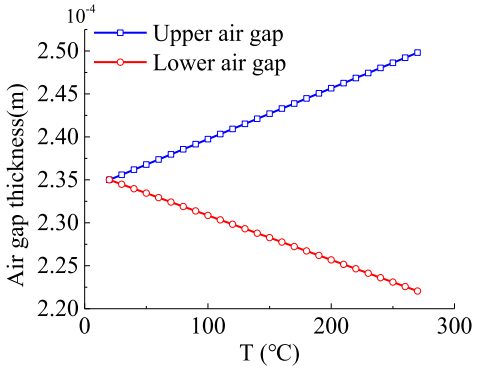

FIGURE 3. Gap's temperature characteristic.

reaches 270°C. Unfortunately, the upper and the lower air gaps have the opposite variation tendency, and then it can be deduced that the temperature rise will destroy the symmetry of the torque motor, which will eventually affect the control precision of the servo valve.

3) CALCULATION OF AIR GAP'S MAGNETIC FLUX

To investigate the effect of temperature variation on the torque motor's driving torque, it is necessary to take each air gap's magnetic flux into account, which is determined by the air gap's reluctance, the polarization magnetomotive force and magnetic flux leakage. Assumptions are given as follows: (a) the flux density of the pole piece and armature will not be saturated; (b) hysteresis of the magnetic circuit is ignored.

Thus, the permanent magnet can be thought to be a magnetic source including a steady magnetomotive force and a reluctance. And the total magnetic flux provided to the external magnetic circuit can be divided into two parts. Part of magnet flux passes through the pole pieces, which is utilized for energy conversion and referred to as the main

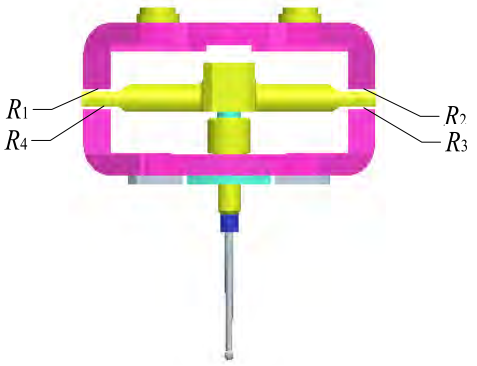

FIGURE 4. Gap reluctances in torque motor.

magnetic flux. And the other magnetic flux is regarded as leaking magnetic flux, whose amount is considerable so that it cannot be ignored. And the proportion of the main magnetic flux, denoted by γ, can be determined by experiments or simulations. Since the magnetic material's reluctances are lower by three orders of magnitude than the air gap's, the effect of the pole pieces and the armature on the magnetic circuit can be ignored. After defining four gap reluctances, depicted in Figure 4, the magnetic circuit of the torque motor can be shown in Figure 5.

Specifically, N_c is the control coils' number of turns, Δi is the current of the control coils, R_0 is the reluctance of the permanent magnet, R_L is the leakage reluctance, ϕ_7 and ϕ_8 are the total fluxes of two permanent magnets, ϕ_1, ϕ_2, ϕ_3, and ϕ_4 are air gap fluxes, ϕ_5 and ϕ_6 are magnetic fluxes of the pole pieces and ϕ_a is the armature flux. And the following equations can be listed by reference to Figure 5.

$$\begin{pmatrix} 1 & 0 & 0 & 0 & 1 & 0 & -\gamma & 0 & 0 \\ 0 & 1 & 0 & 0 & -1 & 0 & 0 & -\gamma & 0 \\ 1 & 0 & 0 & -1 & 0 & 0 & 0 & 0 & -1 \\ 0 & 1 & -1 & 0 & 0 & 0 & 0 & 0 & 1 \\ 0 & 0 & 1 & 0 & 0 & -1 & 0 & -\gamma & 0 \\ R_1 & 0 & 0 & R_4 & 0 & 0 & R_0 & 0 & 0 \\ 0 & R_2 & R_3 & 0 & 0 & 0 & 0 & R_0 & 0 \\ R_1 & -R_2 & 0 & 0 & 0 & 0 & 0 & 0 & 0 \\ 0 & 0 & R_3 & -R_4 & 0 & 0 & 0 & 0 & 0 \end{pmatrix} \begin{pmatrix} \phi_1 \\ \phi_2 \\ \phi_3 \\ \phi_4 \\ \phi_5 \\ \phi_6 \\ \phi_7 \\ \phi_8 \\ \phi_a \end{pmatrix} = \begin{pmatrix} 0 \\ 0 \\ 0 \\ 0 \\ 0 \\ M_0 \\ M_0 \\ N_c\Delta i \\ N_c\Delta i \end{pmatrix} \tag{11}$$

Considering the influence of temperature on the length and the sectional area, the reluctance R_0 in Eq. (11) is calculated

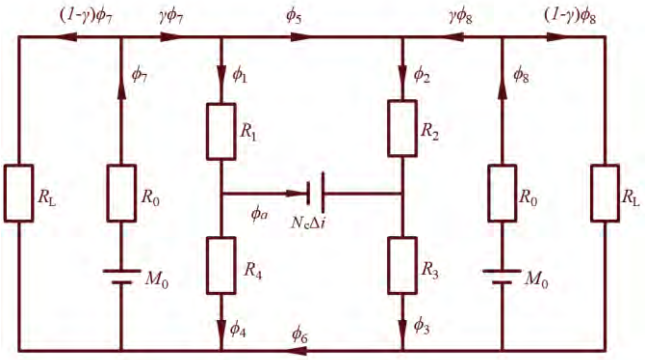

FIGURE 5. Magnetic circuit of torque motor.

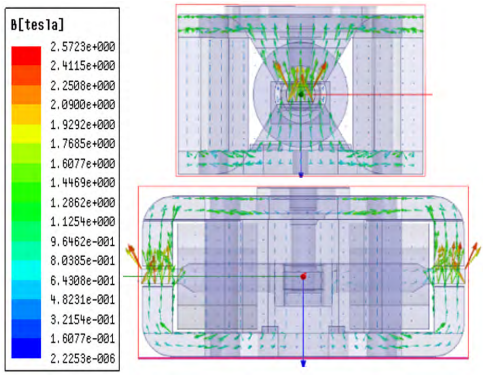

FIGURE 6. Distribution of Magnetic fluxes.

by

$$R_0 = \frac{l_m\,(1+\alpha_m\Delta T)}{\mu_r A_m\,(1+2\alpha_m\Delta T)} \tag{12}$$

where A_m is the sectional area of the permanent magnet. And the expressions of the four air gaps' reluctances are

$$\begin{cases} R_1 = \dfrac{l_{g1}-x}{\mu_0 A_g}, & R_2 = \dfrac{l_{g1}+x}{\mu_0 A_g} \\ R_3 = \dfrac{l_{g2}-x}{\mu_0 A_g}, & R_4 = \dfrac{l_{g2}+x}{\mu_0 A_g} \end{cases} \tag{13}$$

in which x is the linear displacement of the armature and A_g is the effective area of each air gas; $A_g = A_{gi}(1+2\alpha_c\Delta T)$.

To verify the above theoretical model of gap fluxes and determine the proportion of effective flux γ, a numerical simulation is carried out. The three-dimensional model of a torque motor is imported into ANSOFT Maxwell framework. Exerting a current excitation on the coil, the distribution of magnetic fluxes of the entire torque motor is shown in Figure 6.

Assuming that $\gamma = 30\%$ by reference to experimental experience, a comparison of theoretical calculation and numerical simulation is made as depicted in Figure 7. When the excitation current varies from 1mA to 10mA at 20°C, the air gap flux of simulating rises approximately linearly, in accordance with calculation by Eq. (11). Thus, the gap

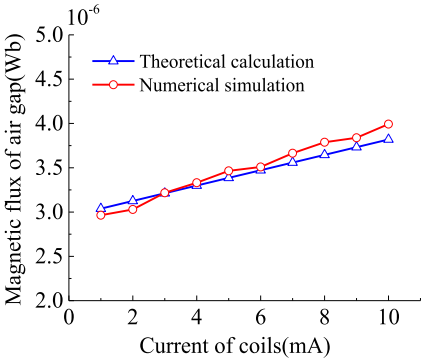

FIGURE 7. Comparison about air gap flux.

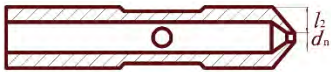

FIGURE 8. Nozzle.

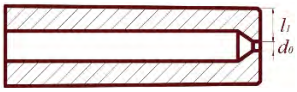

FIGURE 9. Fixed orifice.

flux model has been proved to be reasonable for the following temperature performance investigating.

B. TEMPERATURE'S EFFECT ON PILOT HYDRAULIC AMPLIFIER AND LOAD DIFFERENTIAL PRESSURE

The actual structure of the nozzle of the hydraulic amplifier and the fixed orifice are displayed in Figs. 8 and 9. The oil with high pressure passes through the fixed orifice and nozzle-flapper orifice, which means that there exist two throttling procedures. The pressure between the two orifices is exerted on the main spool.

The temperature's rise will have an effect on these tiny throttling elements. Both the nozzle and the fixed orifice are assembled with interference fit, so it can be assumed that the material expands towards inside as temperature rises. With the same material, the diameter of the two orifices can be calculated by

$$\begin{cases} d_n = d_{ni} - 2l_2\alpha_p\Delta T \\ d_0 = d_{0i} - 2l_1\alpha_p\Delta T \end{cases} \tag{14}$$

where α_p is the expansion coefficient of the nozzle material; d_{ni} and d_{0i} are the diameters of the nozzle and the fixed orifice at the initial temperature, respectively.

Additionally, even if there is no torque motor's deflection, the gap between the nozzle and the flapper, as shown in Figure 10, is affected by material expansion. At the initial temperature, the thickness of the gap, the flapper thickness and the free end's length are denoted by x_{f0i}, L_{1i} and L_{2i}, respectively. Considering that the material of the flapper is the same as that of the nozzle, with temperature variation the

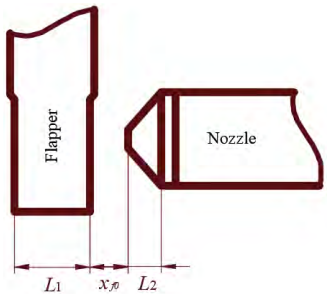

FIGURE 10. Nozzle and flapper.

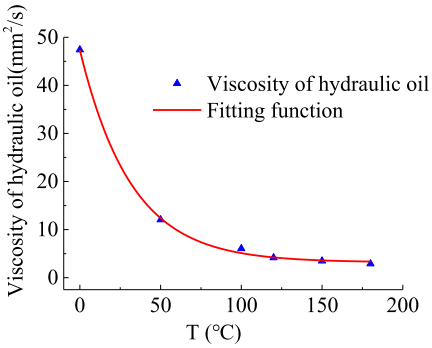

FIGURE 11. Viscosity as a function of temperature.

gap's thickness x_{f0} can be computed by

$$x_{f0} = x_{f0i} - \alpha_p \left(\frac{L_{1i}}{2} + L_{2i} \right) \cdot \Delta T \tag{15}$$

Thermal-solid coupling simulations based on the finite element model of the fixed orifice and the nozzle-flapper structure are performed. It is showed that as temperature rises the orifice material expands towards inside and the nozzle expands towards the flapper. And the deformation is consistent with the theoretical calculation.

The nozzle and the gap constitute a combined orifice, which is referred to as the nozzle-flapper orifice and will cooperate with the fixed orifice. If the main spool is stationary and leakage is not taken into account, the flow through the two orifices will be continuous so that

$$\begin{cases} \dfrac{\pi d_0^2}{4} C_{d0} \sqrt{\dfrac{2}{\rho}(p_s - p_1)} \\ \qquad = C_{df} \pi d_n \left(x_{f0} - x_f \right) \sqrt{\dfrac{2}{\rho}(p_1 - p_0)} \\ \dfrac{\pi d_0^2}{4} C_{d0} \sqrt{\dfrac{2}{\rho}(p_s - p_2)} \\ \qquad = C_{df} \pi d_n \left(x_{f0} + x_f \right) \sqrt{\dfrac{2}{\rho}(p_2 - p_0)} \end{cases} \tag{16}$$

where C_{d0} is the flow coefficient of the fixed orifice, C_{df} is the flow coefficient of the nozzle-flapper orifice, p_1 and p_2 are pressures between the two orifices on both sides, p_s and p_0 are the supply pressure and the back pressure, and x_f is flapper's displacement.

To obtain flow coefficients at different temperatures, the effect of temperature variation on the viscosity is firstly considered. According to the Reynolds viscosity-temperature formula [22], [8], the viscosity of hydraulic oil is phrased as

$$v = v_i e^{-\lambda \Delta T} \tag{17}$$

where v_i is the viscosity at the initial temperature and λ is the viscosity-temperature coefficient. By reference to Eq. (17) and viscosity data of 12# aeronautical hydraulic oil listed in Ref. [8], we can obtain the fitting function

$$v = 48.46 e^{-0.03 \Delta T} \text{mm}^2/\text{s} \tag{18}$$

as depicted in Figure 11.

Consider the flow coefficient at different temperatures. As described by [21], CFD simulation is an important means to analyze the flow coefficient of hydraulic valves. According to parameters resulting from (14), (15) and (17) at different temperatures, a three-dimensional numerical model is built, as shown in Figure 12a.

Specifically, the inlet pressure is specified at 15Mpa and the outlet at 3Mpa, similar to actual scenarios. And all the other surfaces are defined as wall boundaries. Assume that the oil is a Newtonian fluid with different viscosities at different temperatures. The Realizable $k - \varepsilon$ turbulence model which is supposed to be effective for flow with both high and low Reynolds number is applied [21]. For low temperature conditions, such as -40°C, a laminar flow is considered. Then the Finite Volume commercial code ANSYS/FLUENT is used to solve the continuity, momentum and turbulence equations, assuming the hypotheses of steady-state and incompressible flow. And a second order upwind spatial discretization scheme is employed.

It follows from the numerical simulation (see Figure 12b) that the flow rate passing the nozzle can be given at different temperatures. Based on the throttling formula, a series of flow coefficients can be computed. Similarly, the same method can be implemented to obtain the flow coefficients of the fixed orifice. Table 3 lists flow coefficients resulting from CFD.

After data fitting according to Table 3, it is found that flow coefficients are exponential functions of temperature variation, that is

$$\begin{cases} C_{df} = -0.00136 e^{-0.1473 \Delta T} + 0.663 \\ C_{d0} = -0.1143 e^{-0.03569 \Delta T} + 0.752 \end{cases} \tag{19}$$

as depicted in Figure 13.

Thus, flow coefficients in the temperature range of -40°C to 150°C are supported directly by simulation data, while at a temperature above 150°C the flow coefficient can be computed according to the fitting function. The calculation shows that maximum errors of C_{df} and C_{d0} are 1.3% and 0.27%, respectively.

As mentioned in [22], the flow coefficients of orifices are determined by the flow regime and the land-length to gap ratio of the nozzle. From 20°C to 270°C the orifice

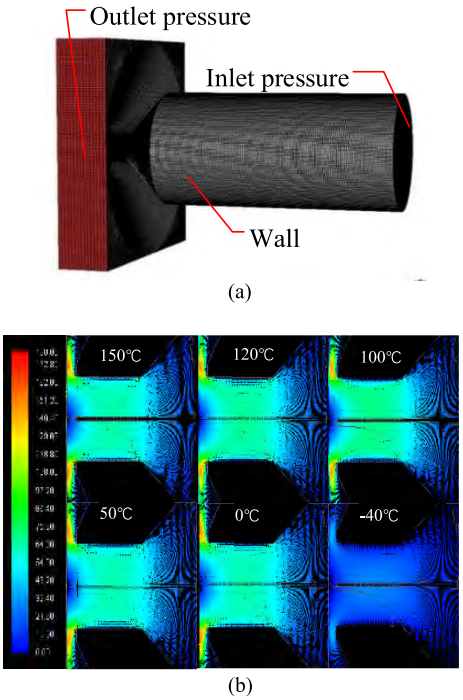

FIGURE 12. (a) CFD model of nozzle-flapper structure. (b) Velocity vector in simulation at different temperatures.

TABLE 3. Flow coefficients at different temperatures from CFD.

Temperature(℃)	Flow coefficient of nozzle-flapper orifice	Flow coefficient of fixed orifice
-40	0.1716	0.2758
-30	0.5501	0.4185
-20	0.6371	0.5186
0	0.6617	0.6372
20	0.6629	0.6960
50	0.6722	0.7348
100	0.6635	0.7467
120	0.6585	0.7509
150	0.6581	0.7517

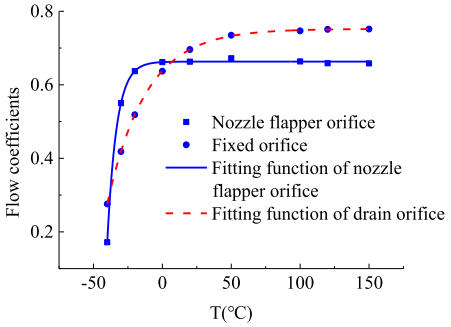

FIGURE 13. Flow coefficients at different temperature.

flow is always turbulent since its Reynolds number materially exceeds the transition Reynolds number; hence the flow coefficient is steady and independent from the Reynolds

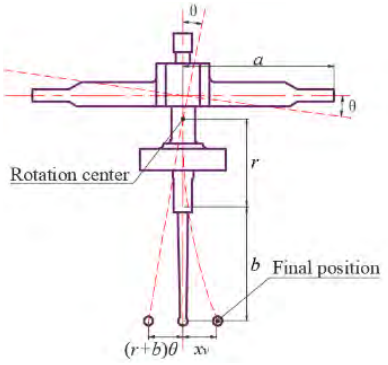

FIGURE 14. Torque motor's geometrical dimensions.

number [22]. Notice that the variation of the gap caused by the deflection of the torque motor is so small, below 2.5% for a current of 1mA. Hence its effect is not considered. In such a scenario, Eq. (19) can be used to calculate the flow coefficient and Eq. (16) holds for different x_f, p_1 and p_2.

Therefore, using Eqs. (14), (15), (16), (18) and (19) gives the pressures at both sides of the main spool.

$$\begin{cases} p_1 = \dfrac{d_0^4 C_{d0}^2 p_s + 16 C_{df}^2 d_n^2 \left(x_{f0} - x_f\right)^2 p_0}{d_0^4 C_{d0}^2 + 16 C_{df}^2 d_n^2 \left(x_{f0} - x_f\right)^2} \\ p_2 = \dfrac{d_0^4 C_{d0}^2 p_s + 16 C_{df}^2 d_n^2 \left(x_{f0} + x_f\right)^2 p_0}{d_0^4 C_{d0}^2 + 16 C_{df}^2 d_n^2 \left(x_{f0} + x_f\right)^2} \end{cases} \tag{20}$$

Introduce the angular displacement of the torque motor θ and the nozzle's arm of force r, as illustrated in Figure 14. Notice that the flapper's displacement $x_f = r\theta$, and then the spool's load differential pressure is

$$p_{Lp} = p_1 - p_2 = \frac{64 d_0^4 C_{d0}^2 C_{df}^2 d_n^2 x_{f0} r\theta \left(p_s - p_0\right)}{\left[d_0^4 C_{d0}^2 + 16 C_{df}^2 d_n^2 \left(x_{f0} - r\theta\right)^2\right]} \times \frac{1}{\left[d_0^4 C_{d0}^2 + 16 C_{df}^2 d_n^2 \left(x_{f0} + r\theta\right)^2\right]} \tag{21}$$

C. MECHANICAL STRUCTURE WITH THE TEMPERATURE VARIATION

1) STIFFNESS OF SPRING TUBE

As shown in Figure 14, the torque motor includes a spring tube and a feedback rod, which will be influenced by the temperature. By reference to Ref. [23], the stiffness of the spring tube can be given by

$$K_s = \frac{\pi E_s \left(D_s^4 - d_s^4\right)}{64 l_s} \tag{22}$$

where D_s is the outer diameter of the spring tube, d_s is the inner diameter of the spring tube, l_s is the length of the spring tube and E_s is the elastic modulus of the material. Consider these parameters' variation. The derivative of the stiffness

with respect to T is expressed as

$$\frac{\partial K_s}{\partial T} = \frac{\pi \partial E_s (D_s^4 - d_s^4)}{64 l_s \partial T} + \frac{4\pi E_s (D_s^3 \partial D_s - d_s^3 \partial d_s)}{64 l_s \partial T} - \frac{\pi E_s \left(D_s^4 - d_s^4\right) \partial l_s}{64 l_s^2 \partial T} \tag{23}$$

The spring tube's material is copper alloy with linear expansion rate α_s, as listed in Table 1. Thus $\Delta l_s/l_s = \Delta D_s/D_s = \Delta d_s/d_s = \alpha_s \Delta T$. And the elastic modulus E_s decreases with the increasing temperature and $\Delta E_s/E_s = -\eta \Delta T$, where η is the temperature coefficient of the elastic modulus. Then (23) can be written as

$$\frac{\Delta K_s}{\Delta T} = \frac{-\pi \eta E_s (D_s^4 - d_s^4)}{64 l_s} + \frac{3\alpha_s \pi E_s \left(D_s^4 - d_s^4\right)}{64 l_s} \tag{24}$$

Following from (24), as temperature rises, thermal dilation increases the stiffness of the spring tube, but the elastic modulus reduces it. In addition, experiments show that α_s/η for the alloy material is approximately 0.04 [24]. Since $\Delta E_s/E_s = -\eta \Delta T$, it follows that $\Delta E_s/E_s = -25\alpha_s \Delta T$. Hence rewrite (24), and we can obtain

$$\frac{\Delta K_s}{\Delta T} \approx \frac{-22\pi \alpha_s E_s \left(D_s^4 - d_s^4\right)}{64 l_s} \tag{25}$$

Consequently, the joint effects of parameters will make the stiffness variation proportional to the linear expansion rate, and the stiffness will decrease with the increase of temperature. Specifically, dimension factors' influences will cancel out each other, slightly increasing the stiffness finally. However, the temperature characteristic of the elastic modulus is the decisive factor causing the total stiffness decline.

Then, the thermal increment rate of spring tube stiffness is defined by

$$\alpha_{K_s} = \frac{\Delta K_s}{K_s \Delta T} = -22\alpha_s \tag{26}$$

Thus the thermal increment rate of the stiffness is more than twenty times of the linear expansion rate of the material. It follows that the stiffness of the spring tube can be expressed as

$$K_s = K_{si} + \Delta K_s = K_{si} \left(1 + \alpha_{K_s} \Delta \mathrm{T}\right) \tag{27}$$

where K_{si} is the stiffness of the spring tube at the initial temperature.

The spring tube plays a stabilizing role on the servo valve. If the installation is not accurate, the torque motor will produce an initial torque and a corresponding displacement θ_i to restore the armature's equilibrium. As temperature rises, the stiffness of the spring tube decreases, θ_i will increase following from $\Delta\theta_i/\theta_i = \Delta K_s/K_s$. For the servo valve, that will be a source of temperature drift.

2) STIFFNESS OF FEEDBACK ROD

According to Ref. [23], the stiffness of the feedback rod can be expressed as

$$K_f = \frac{3E_f \pi D_f^3 d_f}{64 L_f^3} \tag{28}$$

in which D_f is the bigger end's diameter of the feedback rod, d_f is the smaller end's diameter, L_f is the length of the deformed segment and E_f is the elastic modulus of feedback rod's material.

Similar to the derivation process for the spring tube, the thermal increment rate of the feedback rod's stiffness is directly listed as follows:

$$\alpha_{K_f} = \frac{1}{K_f}\frac{\partial K_f}{\partial T} = \frac{1}{K_f}\left[\frac{3\partial E_f \pi D_f^3 d_f}{64 L_f^3 \partial T} + \frac{9E_f \pi D_f^2 \partial D_f d_f}{64 L_f^3 \partial T} + \frac{3E_f \pi D_f^3 \partial d_f}{64 L_f^3 \partial T} + \frac{9E_f \pi D_f^3 d_f \partial L_f}{64 L_f^4 \partial T}\right] \tag{29}$$

and we can obtain

$$\alpha_{K_f} = \frac{\Delta E_f}{E_f \Delta T} + \frac{3\Delta D_f}{D_f \Delta T} + \frac{\Delta d_f}{d_f \Delta T} - \frac{3\Delta L_f}{L_f \Delta T} = -24\alpha_f \tag{30}$$

where α_f is the linear expansion rate of the feedback rod, with a value listed in Table 1.

Still, the temperature characteristic of the elastic modulus is the decisive factor, which causes a decrease of the stiffness at a greater rate than the spring tube. The stiffness of the feedback rod is written as

$$K_f = K_{fi} \left(1 + \alpha_{K_f} \Delta T\right) \tag{31}$$

where K_{fi} is the feedback rod's stiffness at the initial temperature.

D. EQUILIBRIUM EQUATIONS OF THE TORQUE MOTOR AND THE SPOOL

The drive torque of the torque motor is generated as

$$T_d = a\left(F_1 + F_3 - F_2 - F_4\right) = \frac{a}{2\mu_0 A_g}\left(\phi_1^2 + \phi_3^2 - \phi_2^2 - \phi_4^2\right) \tag{32}$$

in which, a is the arm of force for exerting torque with $a = a_i\left(1 + a_c \Delta T\right)$, where a_i is the value at the initial temperature. And F_1, F_2, F_3 and F_4 are electromagnetic forces of four air gaps. A_g is the air gap's effective area.

On the other hand, when the torque motor is in steady state or moves slowly, the moment equilibrium equation is described by

$$T_d = K_s\theta + (r+b) K_f \left[(r+b)\theta + x_v\right] + r p_{Lp} A_N - 8\pi r^2 C_{df}^2 x_{f0} p_s \theta \tag{33}$$

where A_N is the nozzle's area.

And for the spool, the force equilibrium equation in steady state is

$$A_v p_{Lp} = K_f \left[(r+b)\theta + x_v\right] + K_f^{'} x_v + F_f \tag{34}$$

TABLE 4. The list of parameters.

Parameters	Numerical value	Unit
L_{1i}	7.05	mm
L_{2i}	7.29	mm
L_{3i}	8.62	mm
L_{4i}	8.85	mm
L_{5i}	2.83	mm
L_{6i}	10.24	mm
L_{7i}	4.22	mm
A_m	7.41	mm^2
μ_0	$4\pi\times10^{-7}$	Wb/m·A
μ_r	$3.47\times4\pi\times10^{-7}$	Wb/m·A
A_{gi}	14.1	mm^2
N_c	2300	
γ	0.3	
d_{0i}	0.22	mm
d_{ni}	0.4	mm
l_1	0.69	mm
l_2	0.55	mm
v_i	4.846×10^{-5}	m^2/s
λ	0.062	
x_{f0i}	0.035	mm
D	0.52	mm
r	7.375	mm
b	13.35	mm
p_s	21	MPa
p_0	14	MPa
a_i	14.15	mm
K_{si}	12.03	N/m
K_{fi}	5184.38	N/m

with $K_f^{'} = 0.43w(p_s - p_{L0})$, that is the stiffness brought by flow force in steady state. A_v is the area of the spool's piston and F_f is the friction of the spool.

E. ANGULAR DISPLACEMENT EQUATION OF TORQUE MOTOR

Based on the above derivation, the torque motor's angular displacement θ is contained in (32), (33), and (34), which implies that there is a coupling of θ and T_d. It follows that θ can be governed by a ninth-order equation as follows:

$$K_9\theta^9 + K_8\theta^8 + K_7\theta^7 + K_6\theta^6 + K_5\theta^5 + K_4\theta^4 + K_3\theta^3 + K_2\theta^2 + K_1\theta + K_0 = 0 \quad (35)$$

where expressions of $K_i(i = 0 \sim 9)$ are listed in Appendix.

As a comprehensive model containing temperature factors, Eq. (35) and each physical parameter's temperature expression derived above can be referred to as the equation of temperature-induced angular drift (TAD). It follows that the mechanism of temperature's acting on the servo valve can be investigated.

The TAD equation includes nonlinear time-variant coefficients and has no analytical solutions, but it can be solved by numerical methods. With the variation in temperature, the coefficients of the equation are impacted on, which will bring an angular drift of the torque motor. In general, calculations show that the coefficients in (35) decrease gradually from higher order to lower order, and the coefficients of the even terms are smaller than those of the odd terms. If we do not consider viscous friction of the spool, K_8 is 0. In addition, variation of the current has a great influence on the coefficients of the even terms and little effect on the odd terms.

IV. DISCUSSION ON THE TAD MODEL

In light of the TAD model above, the air gaps' thicknesses, the permanent magnets' reluctances, the polarization magnetomotive force, the size of the orifice, the flow coefficient, the stiffness of the spring tube, the stiffness of the feedback rod and the armature's arm of force are temperature-sensitive and as a result the temperature variation will affect control precision of the servo valve by them. To investigate the acting mechanism of the temperature, these main routes of temperature action are taken into account separately. Exerting a current of 1mA on the TAD model, calculations are carried out in the temperature range of 20°C to 270°C, using parameters listed in Tables 1, 2, 3 and 4. And calculation results are given by Figure. 15.

It follows from Figs. 15a and 15c that the influences of temperature fluctuation on the angular drift through the flow coefficient and the air gap thickness are nonlinear. Specifically, the drift tendency caused by flow coefficients has a correlation with the viscosity-temperature property of hydraulic oil illustrated by Figure 11. And the angle variation related to air gaps' thicknesses is an approximate parabolic function. However, through other routes temperature's effects on the angular displacement are linear. Among them, the polarization magnetomotive force, the nozzle orifice's size, the spring tube's stiffness and the feedback rod's stiffness give the angular drifts in the same direction, depicted in Figure 15b, while the armature's radius and the permanent magnets' reluctances have the contrary influence, depicted in Figure 15a, which will play a negative role in the control error in reality.

Consider the control error brought by temperature variation. Relative to the initial operating point (20°C), the temperature-induced angular drift by the flow coefficient of the nozzle is largest, with a maximum of 16.01%. While through the nozzle orifice's size and the polarization magnetomotive force, the temperature's influence is smaller, with maximum errors of 2.88% and 3.168%, respectively. The other effects are slight, that is, by the air gaps' thicknesses the error is 0.9648%, by the permanent magnets' reluctances it is 0.163%, by the armature's arm of force it is 0.163%, by the spring tube's stiffness it is 0.700%, and by the feedback rod's stiffness it is 0.065%. Figure 16 illustrates a comparison of maximum control errors induced by temperature variation through different routes.

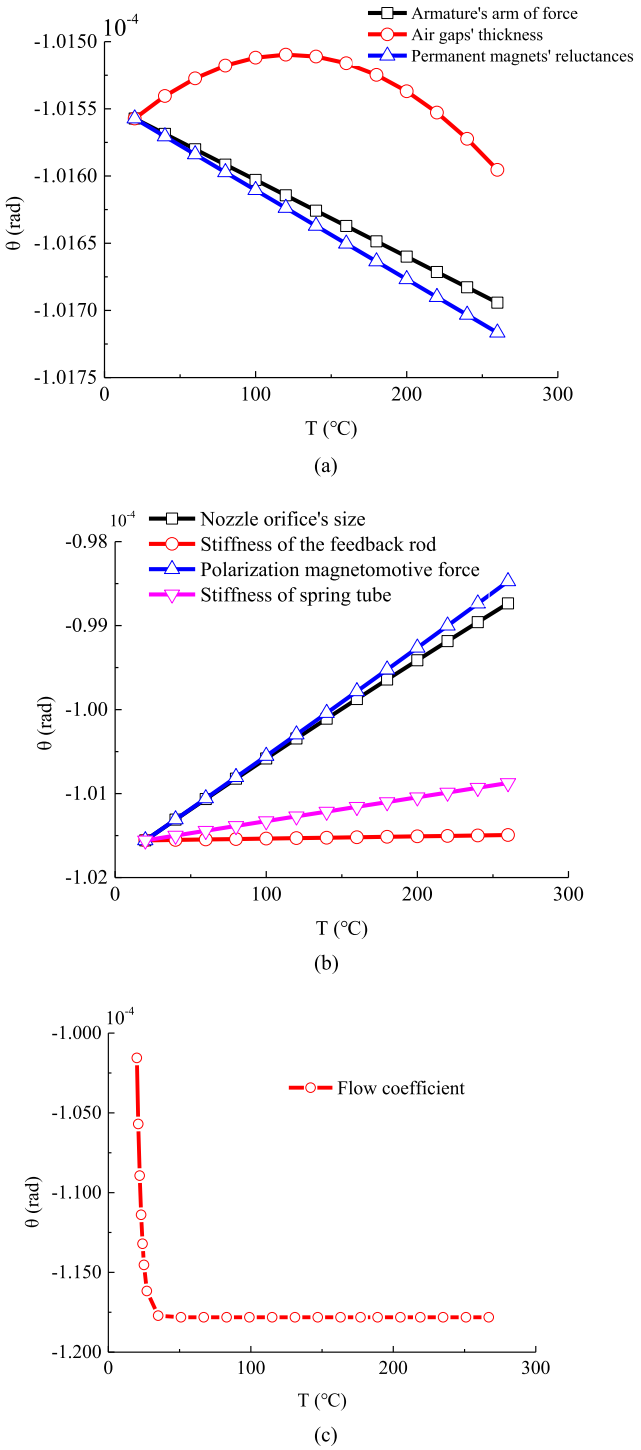

FIGURE 15. (a) Angular temperature-induced drifts by part of routes. (b) Angular temperature-induced drifts by part of routes. (c) Angular temperature-induced drift by flow coefficient.

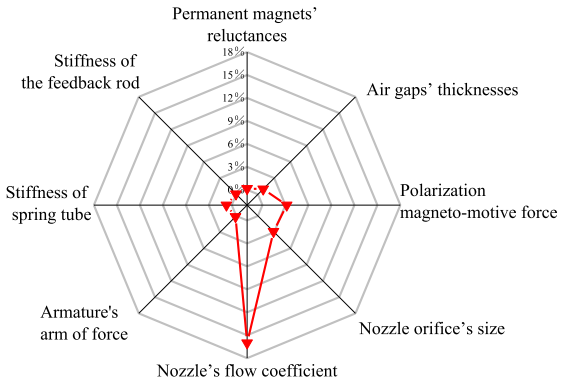

FIGURE 16. Angular errors brought by temperature by different routes.

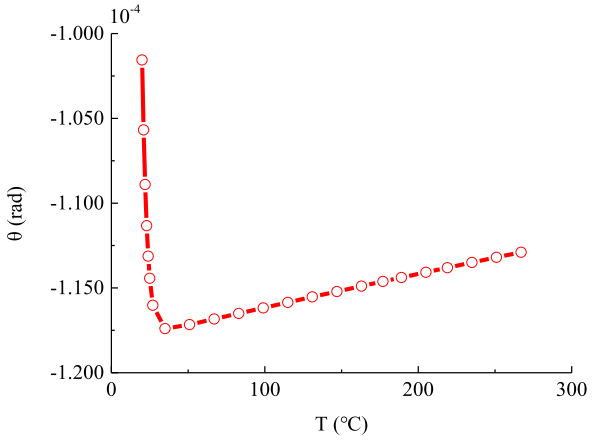

FIGURE 17. Comprehensive influence of temperature rise on the control error.

According to the above analyses, the TAD model exhibits a great nonlinearity so that the total effect of the temperature on the servo valve is not a superposition of the effects from different routes. Assume that the valve has a uniform temperature distribution since there is little difference in temperature between parts of the servo valve when it reaches thermal equilibrium and the temperature of supplied oil is in steady state [4]. Hence, the overall error brought by temperature rise can be computed by Eq. (35), with the result displayed in Figure 17.

It follows that the angular drift of the torque motor increases sharply when the temperature ranges from 20°C to 40°C, but the angle will gradually recover at a low rate when the temperature is beyond 40°C. Within the range of 20°C to 270°C the maximum angular error is 15.6%. Consequently, it can be deduced that the viscosity factor at lower temperature can significantly influence the control precision. When the temperature exceeds a certain value, the viscosity of hydraulic oil become stable, and then other factors will gradually weaken the negative effect of viscosity.

Moreover, the effects of the temperature with different excitation currents are investigated and the calculation results are shown in Figure 18. Hence a consistence for different current is reflected. The maximum control errors caused by temperature are all 15.6%. Correspondingly, with the larger driving signal, the recovery phenomenon is more remarkable.

V. EXPERIMENTAL METHODOLOGY AND RESULT

To construct a suitable temperature condition for evaluating the effect of temperature on the servo valve experimentally,

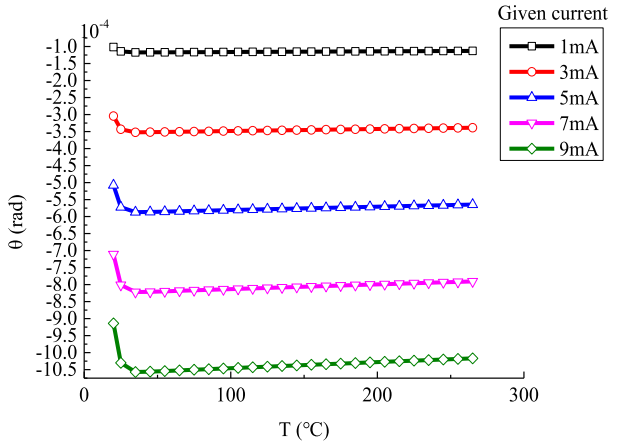

FIGURE 18. Angular drifts for different driving currents.

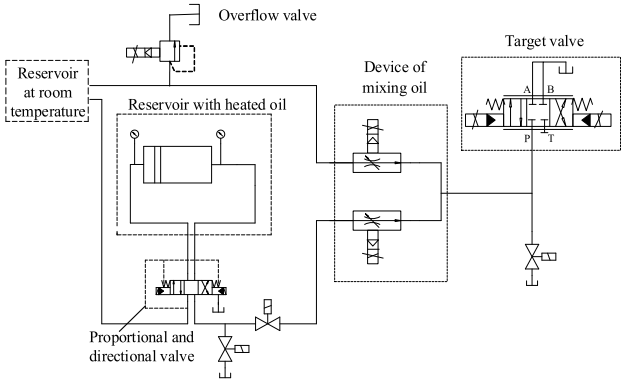

FIGURE 19. Hydraulic oil's temperature control system.

FIGURE 20. Device of mixing oil.

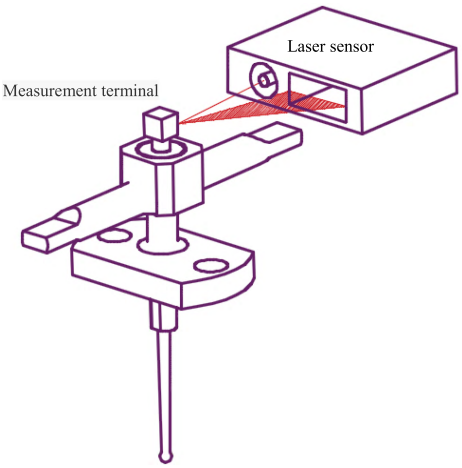

FIGURE 21. Detecting method of angular drift.

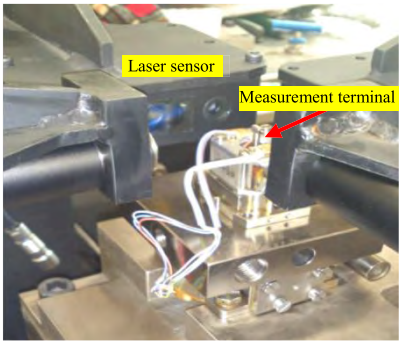

FIGURE 22. Special experimental device.

TABLE 5. Parameters experimental device.

Parameters	Numerical value	Unit
Maximum flow rate	20	L/min
Rated pressure	31.5	MPa
Maximum pressure	35	MPa
Working temperature	0~100	°C
Maximum current of valve	±15	mA

a temperature control system was established, as illustrated in Figure 19. By mixing oil at a high temperature of 200°C and oil at normal room temperature in different proportions by two pneumatic throttling valves, as displayed in Figure 20, the temperature of oil fed to the servo valve is controlled. In order to guarantee the temperature uniformity of the servo valve, a low rate of temperature adjusting is designated. The experimental temperature is limited to a maximum of 95°C.

Since the armature's deflection angle is tiny, it needs to be acquired indirectly, and the detecting method is shown in Figure 21. A terminal block for measurement is fixed above the armature, and its displacement is detected by a laser sensor. Therefore, the angular drift of the torque motor can be computed by reference to the geometry. The experimental device is exhibited by Figure 22 and its parameters are shown in Table 5.

In the experiment, a current of 1mA was given to the two coils of the servo valve, and the angle deflection of the torque motor was monitored through the terminal block. Because the highest working temperature of the experimental device was 100°C, the oil was heated from 20°C to 95°C. From the experimental result, as shown in Figure 23, it can be seen that the actual temperature variation has the same tendency of influencing the angular drift as the theoretical calculation, which confirms the validity of the proposed TAD model. Hence the internal mechanism of leading to the emergence of experimental phenomena can be explained by the TAD

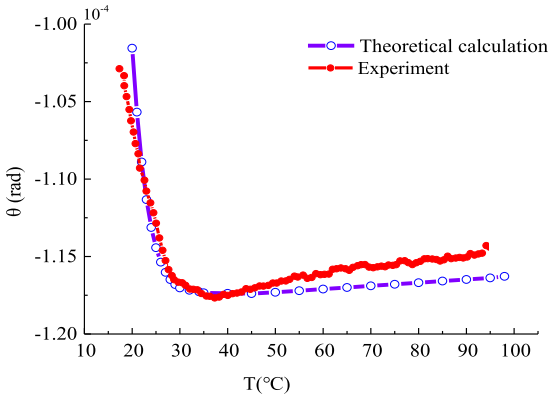

FIGURE 23. Experiment result.

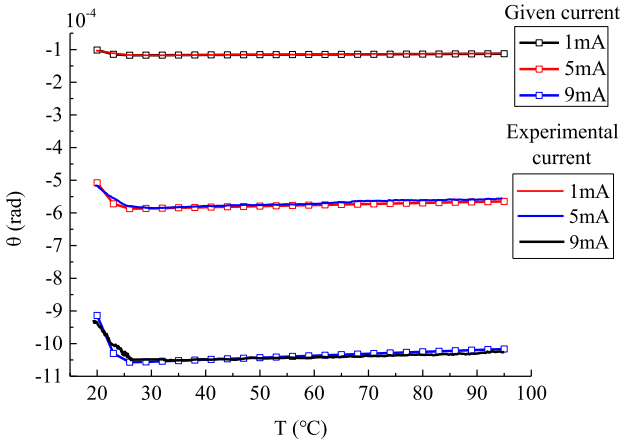

FIGURE 24. Experiment result in different current.

model. At high temperature the angle deviates slightly in the recovery phase, which is supposed to be related to manufacturing errors and inaccuracy of material parameters. If a larger current is given, this angle deviation becomes more remarkable, as shown in Fig. 24. However, since servo valves often work near the zero position, the scenarios with small currents are more representative.

VI. CONCLUSION

Temperature can affect the control precision through multiple routes, which brings different effects on the servo valve. With a mutual coupling, these effects jointly determine the ultimate temperature characteristics of the servo valve. The calculation based on the TAD model and the experiment show that the control error of the torque motor increases sharply and then recovers slowly within the temperature range of 20°C to 270°C. And the maximum angular drift can exceed 15%, which has a significant influence on the servo valve.

Among these temperature's acting routes, the flow coefficient is the dominant route and leads to the largest temperature-induced error. However, it happens just while the temperature varies from 20°C to 40°C, which is correlative of the viscosity-temperature characteristic of hydraulic oil. And through the air gaps' thicknesses and the flow coefficient the temperature's effect is nonlinear, while it is linear for other routes. And the polarization magnetomotive force, the nozzle orifice's size, the spring tube's stiffness, and the feedback rod's stiffness can weaken the temperature-induced drift, while the armature's arm of force and the permanent magnets' reluctances will play a negative role.

The TAD model is an open research framework. For the temperature shock exerted on the servo valve, it is available to consider the dynamic temperature distribution in this model, and the mechanism of the temperature's acting on the servo valve can be described more accurately, which will provide new opportunities of improving the servo valve's performance.

APPENDIX

$$
\begin{aligned}
K_9 &= a_4c_4,\\
K_8 &= A_1b_4c_4 + A_3a_4c_4,\\
K_7 &= A_1b_3c_4 + a_4c_2 + a_2c_4,\\
K_6 &= A_1\left(b_4c_2 + b_2c_4\right) + A_3\left(a_4c_2 + a_2c_4\right),\\
K_5 &= A_1\left(b_3c_2 + b_1c_4\right) + A_2a_4d_1 + a_4c_0 + a_2c_2 + a_0c_4,\\
K_4 &= A_1\left(b_4c_0 + b_2c_2 + b_0c_4\right) + A_3\left(a_4c_0 + a_2c_2 + a_0c_4\right),\\
K_3 &= A_1\left(b_3c_0 + b_1c_2\right) + A_2a_2d_1 + a_2c_0 + a_0c_2,\\
K_2 &= A_1\left(b_2c_0 + b_0c_2\right) + A_3\left(a_2c_0 + a_0c_2\right),\\
K_1 &= A_1b_1c_0 + A_2a_0d_1 + a_0c_0,\\
K_0 &= A_1b_0c_0 + A_3a_0c_0.
\end{aligned}
$$

where

$$
\begin{aligned}
b_2 &= aA_g\mu_0 \times \left(2a^2\Delta i\gamma^2 l_{g1}^2 M_0N_c + 4a^2\Delta i\gamma^2 l_{g1}l_{g2}M_0N_c\right.\\
&\quad \left.+2a^2\Delta i\gamma^2 l_{g2}^2 M_0N_c\right),\\
b_1 &= aA_g\mu_0 \times (4a\gamma^2 l_{g1}^2 l_{g2}M_0^2 + 4a\gamma^2 l_{g1}l_{g2}^2 M_0^2\\
&\quad + a\Delta i^2\gamma^2 l_{g1}^3 N_c^2 + 3a\Delta i^2\gamma^2 l_{g1}^2 l_{g2}N_c^2\\
&\quad + 3a\Delta i^2\gamma^2 l_{g1}l_{g2}^2 N_c^2 + a\Delta i^2\gamma^2 l_{g2}^3 N_c^2\\
&\quad + aA_g\Delta i^2\gamma l_{g1}^2\mu_0 N_c^2R_0 + 2aA_g\Delta i^2\gamma l_{g1}\mu_0 N_c^2R_0\\
&\quad + aA_g\Delta i^2\gamma l_{g2}^2\mu_0 N_c^2R_0),\\
b_0 &= aA_g\mu_0 \times (2\Delta i\gamma^2 l_{g1}^3 l_{g2}M_0N_c + 4\Delta i\gamma^2 l_{g1}^2 l_{g2}^2 M_0N_c\\
&\quad + 2\Delta i\gamma^2 l_{g1}l_{g2}^3 M_0N_c + 2A_g\Delta i\gamma l_{g1}^2 l_{g2}M_0\mu_0 N_cR_0\\
&\quad + 2A_g\Delta i\gamma l_{g1}l_{g2}^2 M_0\mu_0 N_cR_0),\\
a_4 &= 2l_{g1}^2a^4\gamma^2 + 4l_{g1}l_{g2}a^4\gamma^2 + 2l_{g2}^2a^4\gamma^2,\\
a_2 &= -4R_0l_{g1}^2l_{g2}a^2\mu_0\gamma A_g - 4R_0l_{g1}l_{g2}^2a^2\mu_0\gamma A_g\\
&\quad - 4l_{g1}^3l_{g2}a^2\gamma^2 - 8l_{g1}^2l_{g2}^2a^2\gamma^2 - 4l_{g1}l_{g2}^3a^2\gamma^2,\\
a_0 &= 2\gamma^2l_{g1}^4l_{g2}^2 + 4\gamma^2l_{g1}^3l_{g2}^3 + 2\gamma^2l_{g1}^2l_{g2}^4 + 4A_g\gamma l_{g1}^3l_{g2}^2\mu_0R_0\\
&\quad + 4A_g\gamma l_{g1}^2l_{g2}^3\mu_0R_0 + 2A_g^2l_{g1}^2l_{g2}^2\mu_0^2R_0^2.\\
c_4 &= 256C_{df}^4d_n^4r^4,\\
c_2 &= 32d_0^4C_{d0}^2C_{df}^2d_n^2r^2 - 512C_{df}^4d_n^4x_{f0}^2r^2\\
c_0 &= 256C_{df}^4d_n^4d_n^4x_{f0}^4 + 32d_0^4C_{d0}^2C_{df}^2d_n^2x_{f0}^2 + d_0^8C_{d0}^4\\
d_1 &= 64d_0^4C_{d0}^2C_{df}^2d_n^2x_{f0}r\left(p_s - p_0\right)
\end{aligned}
$$

$$A_1 = \frac{K_f + K_f^{'}}{\left(K_f + K_f^{'}\right)\left[K_a + K_f\,(r+b)^2 - 8\pi r^2 C_{df}^2 p_s x_{f0}\right] - K_f^2\,(r+b)^2}$$

$$A_2 = \frac{-rA_N(K_f + K_f^{'}) - K_f\,(r+b)\,A_v}{\left(K_f + K_f^{'}\right)\left[K_a + K_f\,(r+b)^2 - 8\pi r^2 C_{df}^2 p_s x_{f0}\right] - K_f^2\,(r+b)^2}$$

$$A_3 = \frac{F_f K_f\,(r+b)}{\left(K_f + K_f^{'}\right)\left[K_a + K_f\,(r+b)^2 - 8\pi r^2 C_{df}^2 p_s x_{f0}\right] - K_f^2\,(r+b)^2}$$

REFERENCES

[1] J. A. Sidders, D. G. Tilley, and P. J. Chappie, "Thermal-hydraulic performance prediction in fluid power systems," *Proc. Inst. Mech. Eng. I, J. Syst. Control Eng.*, vol. 210, no. 4, pp. 231–242, 1996.

[2] T. E. Green and J. R. Snell, "Thermographic inspection of hydraulic systems," *Proc. SPIE*, vol. 2766, pp. 25–30, Mar. 1996.

[3] W. Zeng, Z. Tong, S. Li, H. Li, and L. Zhang, "Thermodynamic characteristic study of a high-temperature flow-rate control valve for fuel supply of scramjet engines," *Chin. J. Aeronaut.*, vol. 25, no. 4, pp. 559–565, 2012.

[4] Y. Zhu, Q. Zhang, J. Tao, D. Tan, and X. Wang, "Heat characteristics analysis of electro-hydraulic servo valve," *J. Thermal Sci. Eng. Appl.*, vol. 11, no. 3, 2018, Art. no. 031008.

[5] Y. Li, B. Li, Y. Shen, and M. Hu, "Thermal-hydraulic modeling and simulation of hydraulic servo valve," *J. Syst. Simul.*, vol. 21, no. 2, pp. 340–343, 2009.

[6] J. Zhao, S. Zhou, X. Lu, and D. Gao, "Numerical simulation and experimental study of heat-fluid-solid coupling of double flapper-nozzle servo valve," *Chin. J. Mech. Eng.*, vol. 28, no. 5, pp. 1030–1038, 2015.

[7] Y. Yin, *Electro Hydraulic Servo Control Theory and Application Technology in Extreme Environment*. Shanghai, China: Shanghai Scientific & Technical, 2012.

[8] Y. Yin, Q. Xiao, and S. Yan, "Influence of temperature on hydraulic servovalve," *Fluid Power Transmiss. Control*, vol. 31, no. 6, pp. 23–26, Nov. 2008.

[9] Q. Xiao, "Characteristics, effect of temperature on electrohydraulic servo valve," M.S. thesis, School Mech. Eng., Tongji Univ., Shanghai, China, 2009.

[10] Z. Xi, Y. Yaobao, and H. Weida, "Influence of temperature on null position pressure characteristics of flapper-nozzle servo valve," in *Proc. Int. Conf. Comput. Design Appl. (ICCDA)*, vol. 3, 2010, pp. 257–261.

[11] Y. Cao, "Temperature rise by Throttling and Thermal deformation of hydraulic valve," M.S. thesis, College Energy Power Eng., Lanzhou Univ. Technol., Gansu, China, 2011.

[12] J. Zhang, X. Kong, and A. I. Chao, "Theory analysis of clamping malfunction for some slide valve," *Hydromechatron. Eng.*, vol. 40, no. 24, pp. 89–95, Dec. 2012.

[13] X. Liu and J. Ke, "CFD research on temperature field in radial clearance of hydraulic spool valve," *Chin. J. Mech. Eng.*, vol. 42, pp. 231–234, May 2006.

[14] J. Yan, J. Ke, H. Liu, D. Zhou, and G. Wang, "Research on fluid-solid-thermal coupling in temperature field of hydraulic slide valves," *China Mech. Eng.*, vol. 25, no. 6, pp. 757–760, 2014.

[15] X. Liu, J. Ke, L. Yu, and G. Wang, "CFD research on temperature field in radial clearance of hydralulic spool valve," *Mach. Tool Hydraul.*, vol. 34, no. 11, pp. 112–114, Nov. 2006.

[16] D. Zhou, H. Liu, J. Qin, K. E. Jian, and J. Yan, "Temperature characteristics study of spool valve based on thermal solid-fluid coupling," *Mach. Tool Hydraul.*, vol. 42, no. 21, pp. 169–171, 2014.

[17] W. Li, "Research of temperature property in hydraulic spool valve," *Hydraulic Pneumatic Seals*, vol. 7, no. 4, pp. 16–19, Dec. 2011.

[18] J. Qin, C. Li, Y. Hao, and L. Lei, "Effect of temperature on torque motor air gap reluctance and permanent magnet polarization magnetomotive force," *Mach. Tool Hydraulic*, vol. 45, no. 9, pp. 105–109, May 2017.

[19] L. Li, C. Li, H. Yan, J. Qin, and P. Wang, "Research on temperature drift current fluctuation of nozzle flapper servo valve," *J. Beijing Jiaotong Univ.*, vol. 41, no. 3, pp. 96–102, 2017.

[20] J. Huang and Z. Guo, *Practical Motor Design and Calculation Manual*. Shanghai, China: Shanghai Scientific & Technical, 2014.

[21] J. R. Valdés, J. M. Rodríguez, J. Saumell, and T. Pütz, "A methodology for the parametric modelling of the flow coefficients and flow rate in hydraulic valves," *Energy Convers. Manag.*, vol. 88, pp. 598–611, Dec. 2014.

[22] H. E. Merritt, *Hydraulic Control Systems*. Hoboken, NJ, USA: Wiley, 1967.

[23] C. Wang, *Hydraulic Servo-System*. Beijing, China: Machinery Industry Press, 1989.

[24] L. Pan, S. Jiao, and X. Du, "The relation between linear expansion coefficient and Yang's modulus of allory materials & temperature at high temperature," *J. Naturnalence Hunan Normalis Univ.*, vol. 23, no. 2, pp. 47–51, Jun. 2000.

HAO YAN received the Ph.D. degree from Harbin Institute of Technology, Harbin, China. He is an Associate Professor with the School of Mechanical, Electronic and Control Engineering, Beijing Jiaotong University, China. His current research interests include mechatronics and parallel mechanism.

YANG LIU is pursuing the M.S. degree in the School of Mechanical, Electronic and Control Engineering, Beijing Jiaotong University, Beijing, China. His current research interest includes electro-hydraulic servo valve.

LI MA received the master's degree in mechatronics from the Tianjin University of Technology, China, in 2017. She is pursuing the Ph.D. degree with the School of Mechanical, Electronic and Control Engineering, Beijing Jiaotong University, Beijing, China. Her current research interests include mechatronics engineering and fluid power transmission and control.